International Refrigeration and Air Conditioning Conference | School of Mechanical Engineering

2021

Steady-State Parametric Study Of Semi-Open Absorption Heat Pump Water Heater Performance

Navin Kumar
Oak Ridge National Laboratory, United States of America, KUMARN1@ORNL.GOV

Kyle R Gluesenkamp
Oak Ridge National Laboratory, United States of America

Zhiyao Yang
Oak Ridge National Laboratory, United States of America

Ahmad Abu-Heiba
Oak Ridge National Laboratory, United States of America

Viral Patel
Oak Ridge National Laboratory, United States of America

See next page for additional authors

Authors
Navin Kumar, Kyle R Gluesenkamp, Zhiyao Yang, Ahmad Abu-Heiba, Viral Patel, Rohit Bhagwat, Sidharth Sanadhya, Richard Rode, Michael Schmid, and Saeed Moghaddam

Steady-State Parametric Study of Semi-Open Absorption Heat Pump Water Heater Performance

Navin KUMAR[1], Kyle R GLUESENKAMP[1*], Zhiyao YANG[1], Ahmad ABU-HEIBA[1], Viral K. PATEL[1], Rohit BHAGWAT[2], Sidharth SANADHYA[2], Richard RODE[2], Michael SCHMID[3], Saeed MOGHADDAM[2]

[1]Oak Ridge National Laboratory, Multifunctional Equipment Integration Group,
Oak Ridge, TN, United States of America
gluesenkampk@ornl.gov

[2]University of Florida, Mechanical Engineering,
Gainesville, FL, United States of America
saeedmog@ufl.edu

[3]Micro Nano Technologies,
Gainesville, FL, United States of America
mschmid@mntusa.com

* Corresponding Author

ABSTRACT

Water heating and dehumidification are major energy consumers in buildings. The novel semi-open absorption heat pump design utilizes the heat of absorption from the dehumidification of space for water heating. The architecture of the system consists of (1) a plate and frame membrane-based absorber, (2) a membrane-based desorber and condenser unit, (3) heat exchangers, (4) ionic liquid, and (5) a 189.3 L (50-gal) water tank. The membrane-based absorber enables heat and mass transfer between three streams: moist air, ionic liquid, and the heat transfer fluid. The heat of vapor absorption elevates the ionic liquid temperature and, in turn, heats the heat transfer fluid. In the desorber unit, the diluted ionic liquid after absorption is heated to above 150°C and reconcentrated. The heat of condensation from the condensation of water vapor in the condenser is utilized for water heating. The dehumidification performance of the absorber directly affects the COP and heating capacity of the system. Understanding the absorber's performance at various operating conditions would allow one to optimize and design a better performing absorber. In this study, the absorber's water heating capacity and performance are evaluated for varying operating conditions. A maximum COP of 1.25 while water heating water from 18.6 to 60.2°C was achieved at a capacity of 1,010 Watts and an airflow rate of 47.19 L/s. Increasing the desorber oil mass flowrate had negligible effect on the COP. The average mass transfer resistance of the porous membrane absorber was 1.164 $*10^{7}$ m/s.

Notice: This manuscript has been authored by UT-Battelle, LLC under Contract No. DE-AC05-00OR22725 with the US Department of Energy. The United States Government retains and the publisher, by accepting the article for publication, acknowledges that the United States Government retains a non-exclusive, paid-up, irrevocable, worldwide license to publish or reproduce the published form of this manuscript, or allow others to do so, for United States Government purposes. The Department of Energy will provide public access to these results of federally sponsored research in accordance with the DOE Public Access Plan (http://energy.gov/downloads/doe-public-access-plan).

1. INTRODUCTION

In recent years, research has been conducted to reduce energy consumption attributed to heating/cooling and water heating in buildings (Abdel-Salam *et al.,* 2014; Ascione *et al.,* 2014; Kolokotsa *et al.,* 2011). Water heating and dehumidification are responsible for a substantial portion of the total energy consumed in a residential building; for instance, water heating and space cooling/heating alone consume 18% (Matulka, 2013) and 16% (U.S. Energy Information Administration, 2020), respectively, of the building total energy consumption.

A potential energy-saving system is an absorption-based heat pump system (Gluesenkamp *et al.*, 2017; Li & Sumathy, 2000) that utilizes the sensible and latent heat from dehumidification for water heating to reduce the total combined energy consumption. Thus, recent studies have focused on environmentally friendly and energy-efficient absorption heat pumps for cooling, water heating, and dehumidification *(*Aman *et al., 2014;* Angrisani *et al., 2017;* Mortazavi *et al.,* 2015). However, the utilization of absorption heat pumps in building appliances was limited by the absorption heat pump system's size, working fluids, and the system's cost (Chugh *et al.,* 2019). However, a recently proposed architecture of a semi-open absorption heat pump, as discussed in (Gluesenkamp *et al.,* 2017), offers a low-cost, efficient, and compact system compared to the existing closed absorption system (Chugh *et al.*, 2017). Compared to a closed system, a semi-open system uses ambient air as a refrigerant, eliminating the need for an evaporator and dehumidifying the air in the process. Recent studies have demonstrated that semi-open absorption water heating could achieve a coefficient of performance (COP) comparable with that of a closed system (Chugh *et al.*, 2017, 2019). The biggest challenge of a semi-open design is the presence of non-condensable gases in the absorber.

In this study, the heat and mass transfer performance of a three-fluid membrane-based plate and frame absorber for water heating is experimentally evaluated and presented. This manuscript provides in-depth details on the experimental set-up used to study absorber performance at varying conditions.

2. EXPERIMENT

Figure 1 shows a schematic of the semi-open absorption heat-pump experimental set-up coupled to two chillers with two water-water heat exchangers (WWHX). The two chillers provide a total water heating load of 1250 Watts, simulating a storage water tank. The ionic liquid (IL) absorbs the water vapor in air through the water vapor permeable membrane (Figure 2). The process water stream flows in the absorber in the counter-flow arrangement and cools the IL as its temperature rises and its concentration decreases while maintaining an isothermal condition. The ionic liquid and process water flow rates are controlled by adjusting a needle valve and the DC pump speed. As the diluted ionic liquid leaves the absorber, it's preheated in the solution-oil heat exchanger (SOHX) before entering the desorber. The diluted ionic liquid is heated above its saturation temperature in the desorber to evaporate the water and re-concentrate it. A circulator heater controls the oil temperature in the desorber and SOHX. The water vapor evaporates off the IL and enters the condenser. The re-concentrated ionic liquid leaves the absorber at a high temperature, enters the solution-water heat exchanger (SWHX), and transfers heat to the process water exiting the absorber. The preheated process water leaving SWHX enters the condenser where it gains heat from the water vapor as it condenses. The heated process water (~ 56°C) leaves the condenser and enters the WWHX. It heats the water from the chiller while maintaining the lowest possible inlet process water temperature to the absorber.

A schematic and photograph of the absorber are shown in Figure 2. The absorber was fabricated with a polycarbonate shell and hydrophobic porous polymeric membrane sheets. Two polycarbonate sheets with machined channels for water flow were thermally-bonded and chemically treated to make the surface hydrophilic. Following the thermal bonding of internal water channels, the polymeric membrane sheets were thermally-bonded to the fins machined on the polycarbonate sheets' reverse side. The fins provided structural support to the membranes and assisted in the mixing of the ionic liquid. The air flows across the membranes through a 3 mm gap between the membrane panels. The properties of the absorber and membrane sheets are summarized in Table 1.

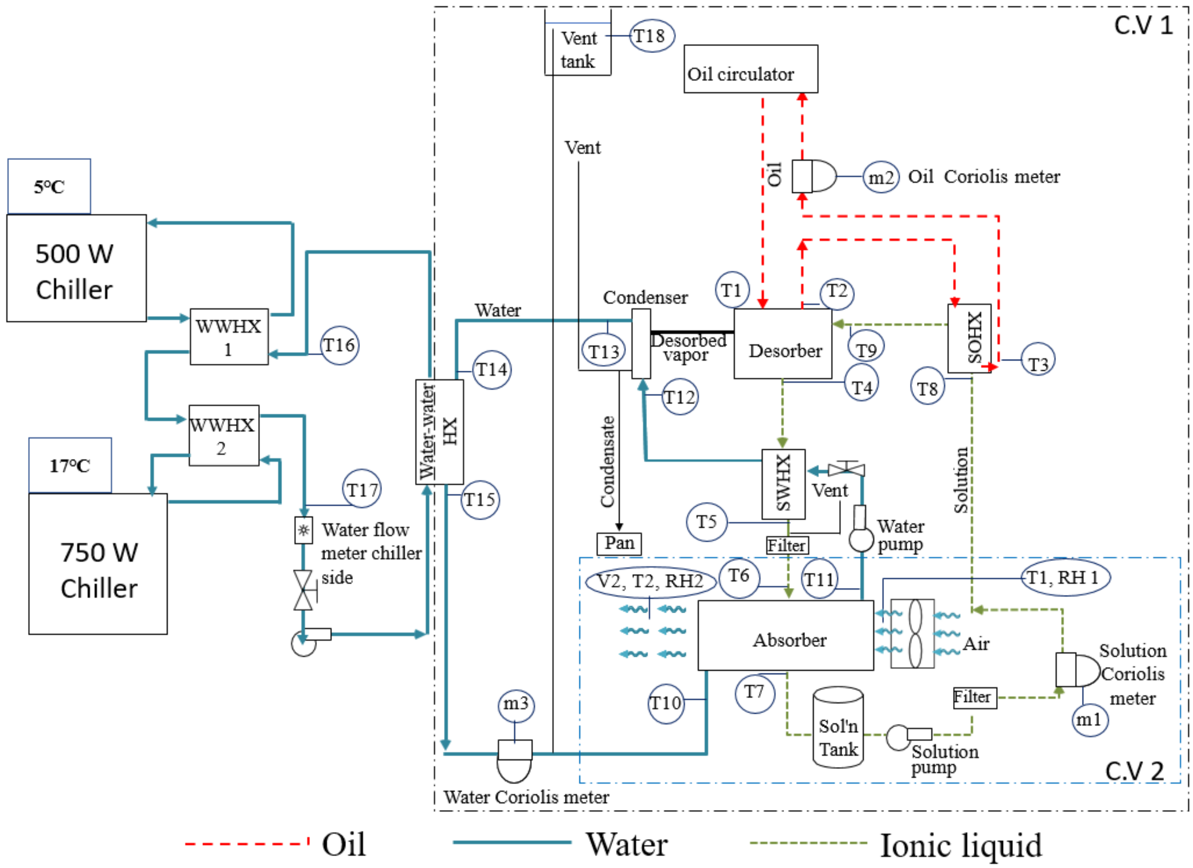

Figure 1: P&ID diagram of the experimental set-up. Control volume 1 (CV 1) analyzes the system level performance; CV 2 analyzes the absorber performance.

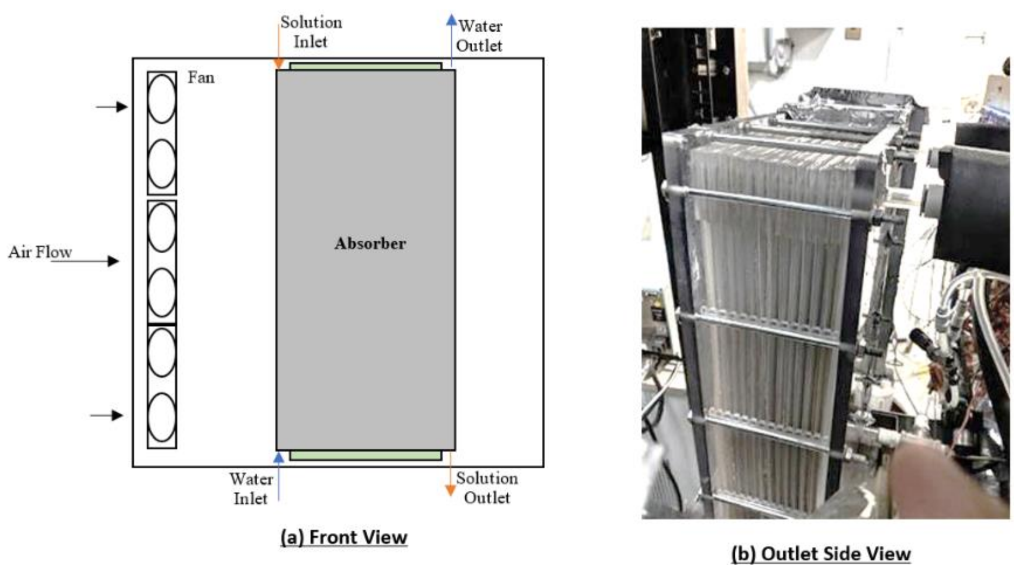

Figure 2: (a) Front view schematic of the absorber. (b) Outlet side view photograph of the absorber.

Table 1: Absorber design properties

Absorber	**This study**
Number of panels	13
Active Surface area (m^2)	1.889
Active plate Volume (m^3)	0.01191
Active surface area/volume ratio (m^{-1})	158.59
Materials used	Polycarbonate and other polymers Thermal and adhesive bonding, CNC machining IL-side fins: 0.6 mm
Membrane pore size	1 µm Thermally bonded on fins

The ionic liquid (IL) in this study was imidazolium methanesulfonate. Chugh *et al.* outlined and summarized the IL thermal properties (Chugh *et al.*, 2017).

The instrument and derived uncertainties are tabulated in Table 2. The derived propagation of uncertainty was computed using Engineering Equation Solver (EES) (Klein, 2016) and Kline & McClintock method (Kline & Mcclintock, 1953). The silicon oil (Boss 470-10) was procured from a manufacturer in USA. The data was acquired using National Instruments DAQ and LabVIEW at 1 Hz sample frequency.

Table 2: Instruments, measurement, and derived uncertainty.

	Quantity	**Instrument**	**Uncertainty**
Measurement	Liquid temperature	T-Type thermocouple	0.5°C
	Mass flow rate (IL, water, oil)	Coriolis mass flowmeter	± 0.5%
	Air relative humidity	Vaisala HMT330	± 0.5 %RH (0 – 40 %RH) ± 0.8 %RH (40 – 95 %RH)
	Air temperature	RTD built into HMT330	0.1°C
	Airflow rate	Differential pressure	± 4%
Derived quantity	COP	N/A	± 3 – 5%
	Q_{total}	N/A	± 1 – 2.5%
	Mass transfer resistance (R_{mt})	N/A	± 8 – 12%

The moisture removal rate (MRR) is the mass of water vapor removed from the air per second and is computed as shown in Eq. 1.

$$MRR = \dot{m}_{air}\left(\omega_{a,in} - \omega_{a,out}\right). \quad (1)$$

Where $\dot{m}_{air}$ is the inlet air mass flowrate, and ω_a is the specific humidity of air at the inlet and outlet of the absorber. The total heating power (Q_{total}) and coefficient of performance (COP) of the semi-open absorption system are computed using Eq. 2 and 3.

$$Q_{total} = Q_{absorber} + Q_{SWHX} + Q_{condenser} = \dot{m_w} \,.\, Cp_w \,.\, [T_{13} - T_{10}] \quad (2)$$

$$COP = \frac{Q_{total}}{Q_{desorber}} = \frac{\dot{m_w} \,.\, Cp_w \,.\, [T_{13} - T_{10}]}{\dot{m_{oil}} \,.\, Cp_{oil} \,.\, [T_1 - T_3]} \quad (3)$$

The absorber's mass transfer resistance (R_{mt}) (Eq. 5) is expressed using the log-mean partial water pressure difference (LMPD) (Eq. 4 and 5), as both the partial vapor pressure of air and solution is varying along the airflow and solution flow direction.

$$LMPD = \frac{(PV_{a,in-} PV_{s,out}) - (PV_{a,out-} PV_{s,in})}{\ln \frac{(PV_{a,in-} PV_{s,out})}{(PV_{a,out-} PV_{s,in})}} \quad (4)$$

$$R_{mt} = \frac{F * LMPD * A_{surf}}{MRR} \quad (5)$$

Due to the cross-flow and three-fluid liquid configuration, Eq. 5 includes a correction factor for cross-flow configuration. The correction factor (F) in this study was between 0.975 and 0.995. The change in the IL vapor pressure at the inlet and outlet was minimal due to the additional cooling. Where PV_a and PV_s are the inlet and outlet solution vapor pressure of the air and solution at the absorber.

3. RESULTS

The total capacity and the COP of the system are presented in Figure 3 as a function of the airside velocity . As the air volumetric flow rate increases, the amount of water vapor transferred from the air to the IL increases, increasing the heat absorption into IL solution. Increasing the air volumetric flow rate reduces the air residence time in the absorber, which in turn reduces the absorber's latent effectiveness.

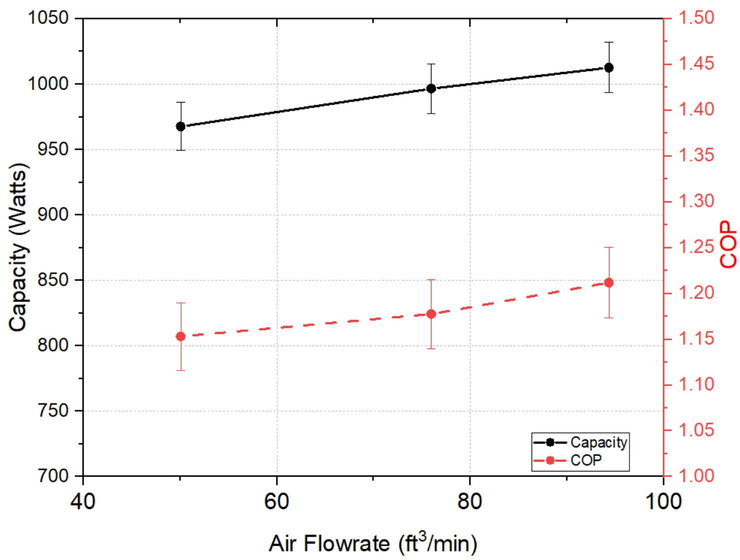

Figure 3: Effect of airflow volumetric flowrate on system COP and capacity. (RH: 49.90 ± 0.8%; T_{air}: 19.88 ± 0.1°C; $\dot{m}_{IL} = 3.0 \pm 0.01$ g/s ; Y_{IL}: 0.853; $\dot{m}_W = 6.0 \pm 0.03$ g/s).

Figure 4 (left) highlights the effect of absorber water inlet temperature on the COP and the system's heating capacity. The heating capacity and COP of the system increase with reducing absorber water inlet temperature. The decrease in the water inlet temperature increases the IL's dehumidification capacity by lowering the IL partial water vapor pressure. Figure 4 (right) highlights the effects of absorber water inlet temperature on the absorber water outlet temperature and system water outlet temperature.

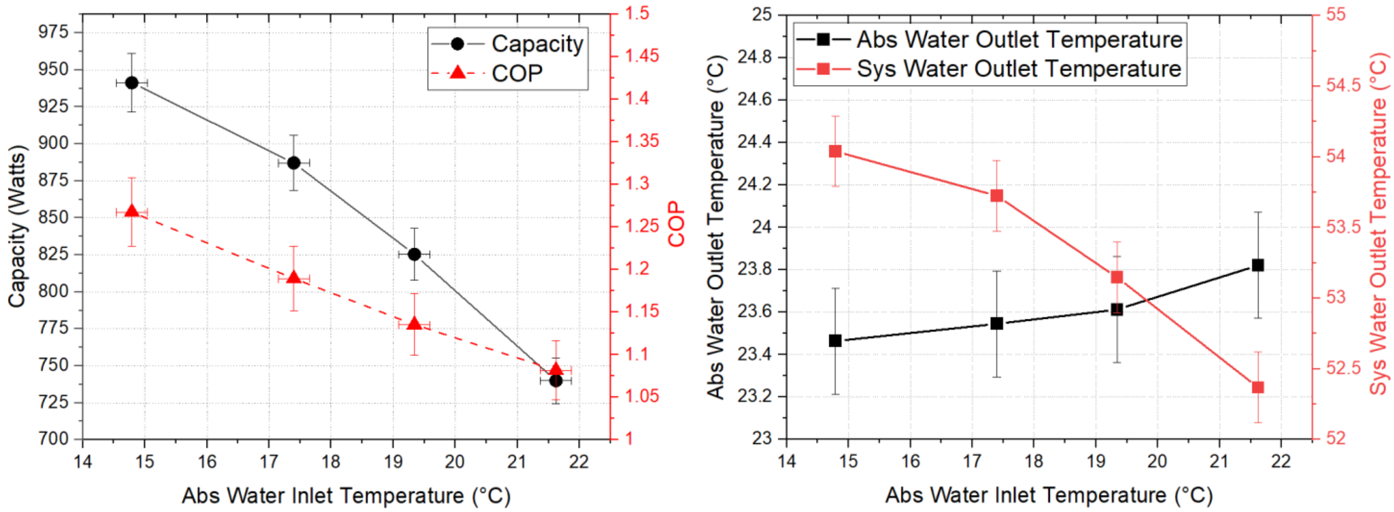

Figure 4: (Left) Effect of absorber (abs) water inlet temperature on system COP and capacity. (Right) Effect of absorber (abs) water inlet temperature on system (system) outlet temperature and absorber outlet temperature. (RH: 49.50 ± 0.8%; T_{air}; 20.00 ± 0.1°C; $\dot{m}_{IL} = 2.5 \pm 0.01$ g/s; Y_{IL}: 0.846; $\dot{m}_W = 5.9 \pm 0.03$ g/s).

Figure 5 highlights the effect of water inlet temperature on the moisture removal rate. The change in moisture removal rate variation was minimum (< 0.0037 g_{vap}/s-m^2) between 14.5 to 19.5°C. Water inlet temperature above 22°C reduced MRR by 33%. Absorber water inlet temperature is an essential design property of the semi-open absorption system. The absorber water inlet temperature is the function of the water heater tank temperature, stratification in the tank, and the load.

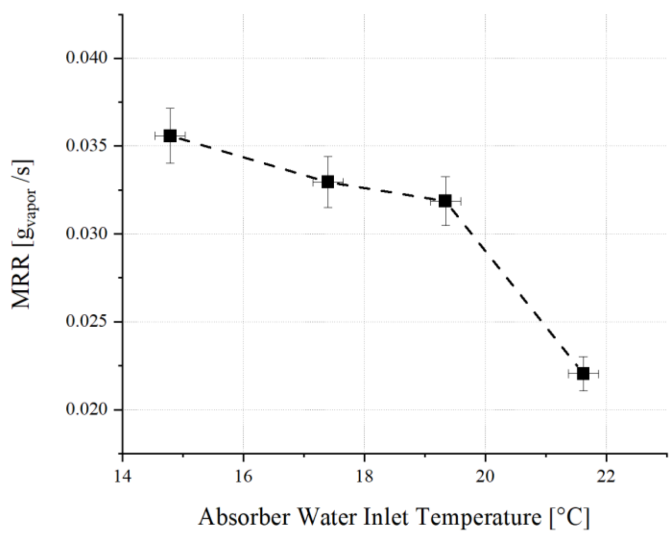

Figure 5: Moisture removal rate (MRR) in this study as a function of the absorber water inlet temperature. (RH: 49.50 ± 0.8%; T_{air}; 20.00 ± 0.1°C; $\dot{m}_{IL} = 2.5 \pm 0.01$ g/s; Y_{IL}: 0.846; $\dot{m}_W = 5.9 \pm 0.03$ g/s).

The effects of oil flowrate and IL solution flowrate on the system capacity and COP are summarized in Figure 6. The heating capacity and COP of the system increases with increasing IL solution flowrate. Increasing the oil mass flow rate increases the system's total heating capacity with negligible effect on the COP. Increasing the oil flowrate from 16 to 46 g/s on average, enhanced the heating capacity by 9.9 %. Increasing the IL solution flow rate from 1.8 to 2.37 g/s improved the heating capacity and COP by 26.6 % and 12.4 %, respectively. Increasing the IL solution flowrate to 3.15 g/s reduced the COP by 3.3 %, while the heating capacity increased by 2.1 %.

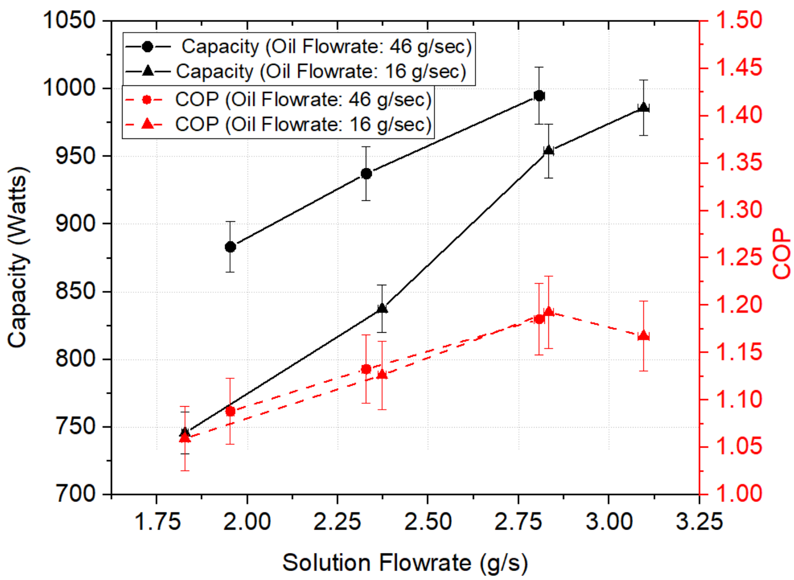

Figure 6: Effect of IL solution and oil flowrate on system COP and Capacity. (RH: 50.20 ± 0.8%; T_{air}; 19.95 ± 0.1°C; Y_{IL}: 0.851; $\dot{m}_W = 5.70 \pm 0.03$ g/s)

The mass transfer resistance was determined experimentally through Eq. 4 and Eq. 5 for porous membranes. The average mass transfer resistance computed over the 19 runs was 1.164 $*10^7$ m/s, with a median absolute deviation of 0.081E7 m/s, as summarized in Figure 7.

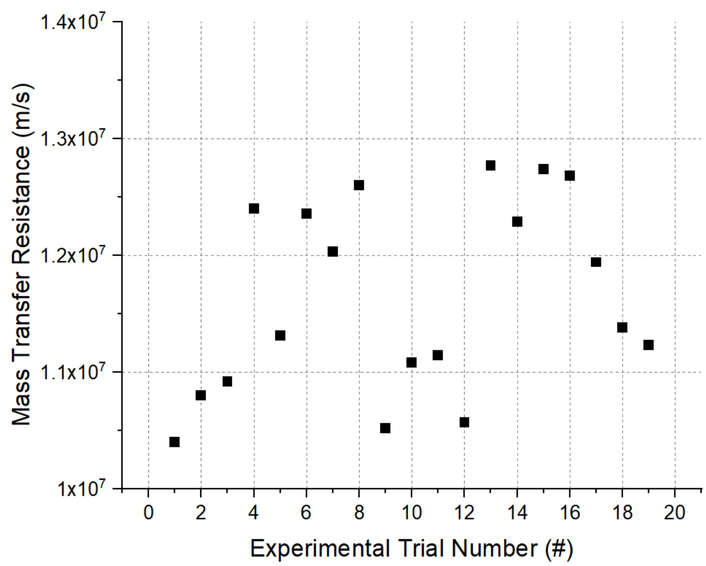

Figure 7: The computed experimental mass transfer resistance of absorber over 19 runs.

4. CONCLUSION

This study highlights a three-fluid membrane-based plate-and frame absorber's performance for water heating and dehumidification for various operating conditions. The parametric study performance on the semi-open membrane-based absorption heat pump highlights that the heating performance and the system's COP are strongly related to the operating conditions.

The following conclusions are drawn from the parametric study performance of the absorber. Doubling the airflow rate only increased the COP and heating capacity by 5.2% and 4.1 % respectively. Increasing the airflow rate reduces the air residence time in the absorber, which reduces the rate of dehumidification. The absorber water inlet temperature significantly impacted the performance of the system. Increasing the water inlet temperature above 19.5°C significantly reduced the MRR, heating capacity, and COP. Increasing the desorber oil mass flowrate increased the heating capacity but had a negligible effect on the COP. The IL flowrate increased the heating capacity and the COP of the system, but the increasing the IL flowrate to 3.12 g/s reduced the COP of system.

NOMENCLATURE

SWHX	Solution - Water Heat Exchanger	
SOHX	Solution – Oil Heat Exchanger	
IL	Ionic Liquid	
COP	Coefficient of Performance	
Y	Mass Fraction	
MRR	Moisture Removal Rate	(g_{vapor}/s-m^2)
RH	Relative Humidity	(%)
T	Temperature	(°C)
Q	Thermal Power	(W)
$\dot{m}$	Mass Flow Rate	(g/s)
ω	Specific Humidity	(g_{vapor}/kg_{air})
Cp	Specific Heat Capacity	(J/g-K)
h	Heat Transfer Coefficient	(m/sec)
Subscripts/Superscripts		
SWHX	Solution - Water Heat Exchanger	
IL	Ionic Liquid	
w	Water	
i	Inlet	
o	Outlet	

REFERENCES

Abdel-Salam, M. R. H., Fauchoux, M., Ge, G., Besant, R. W., & Simonson, C. J. (2014). Expected energy and economic benefits, and environmental impacts for liquid-to-air membrane energy exchangers (LAMEEs) in HVAC systems: A review. *Applied Energy*, *127*, 202–218. https://doi.org/10.1016/j.apenergy.2014.04.004

Aman, J., Ting, D. S.-K., & Henshaw, P. (2014). Residential solar air conditioning: Energy and exergy analyses of an ammonia–water absorption cooling system. *Applied Thermal Engineering*, *62*(2), 424–432. https://doi.org/10.1016/j.applthermaleng.2013.10.006

Angrisani, G., Canelli, M., Roselli, C., Russo, A., Sasso, M., & Tariello, F. (2017). A small scale polygeneration system based on compression/absorption heat pump. *Applied Thermal Engineering*, *114*, 1393–1402. https://doi.org/10.1016/j.applthermaleng.2016.10.048

Ascione, F., Bianco, N., De Masi, R. F., de' Rossi, F., & Vanoli, G. P. (2014). Energy refurbishment of existing buildings through the use of phase change materials: Energy savings and indoor comfort in the cooling season. *Applied Energy*, *113*, 990–1007. https://doi.org/10.1016/j.apenergy.2013.08.045

Chugh, D., Gluesenkamp, K., Abdelaziz, O., & Moghaddam, S. (2017). Ionic liquid-based hybrid absorption cycle for water heating, dehumidification, and cooling. *Applied Energy*, *202*, 746–754. https://doi.org/10.1016/j.apenergy.2017.05.161

Chugh, D., Gluesenkamp, K. R., Abu-Heiba, A., Alipanah, M., Fazeli, A., Rode, R., Schmid, M., Patel, V. K., & Moghaddam, S. (2019). Experimental evaluation of a semi-open membrane-based absorption heat pump system utilizing ionic liquids. *Applied Energy*, *239*, 919–927. https://doi.org/10.1016/j.apenergy.2019.01.251

Gluesenkamp, K. R., Chugh, D., Abdelaziz, O., & Moghaddam, S. (2017). Efficiency analysis of semi-open sorption heat pump systems. *Renewable Energy*, *110*, 95–104. https://doi.org/10.1016/j.renene.2016.07.075

Klein, S. . (2016). Engineering Equation Solver. In *F-Chart Software*.

Kline, S., & Mcclintock, F. (1953). Describing Uncertainties in Single-Sample Experimentstle. *Mechanical Engineering*, *75*, 3–8.

Kolokotsa, D., Rovas, D., Kosmatopoulos, E., & Kalaitzakis, K. (2011). A roadmap towards intelligent net zero- and positive-energy buildings. *Solar Energy*, *85*(12), 3067–3084. https://doi.org/10.1016/j.solener.2010.09.001

Li, Z. ., & Sumathy, K. (2000). Technology development in the solar absorption air-conditioning systems. *Renewable and Sustainable Energy Reviews*, *4*(3), 267–293. https://doi.org/10.1016/S1364-0321(99)00016-7

Matulka, R. (2013). *New Infographic and Projects to Keep Your Energy Bills Out of Hot Water*. Department of Energy. https://www.energy.gov/articles/new-infographic-and-projects-keep-your-energy-bills-out-hot-water

Mortazavi, M., Nasr Isfahani, R., Bigham, S., & Moghaddam, S. (2015). Absorption characteristics of falling film LiBr (lithium bromide) solution over a finned structure. *Energy*, *87*, 270–278. https://doi.org/10.1016/j.energy.2015.04.074

U.S. Energy Information Administration. (2020). *Residential Sector Key Indicators and Consumption*. ANNUAL ENERGY OUTLOOK 2020. https://www.eia.gov/outlooks/aeo/

ACKNOWLEDGMENTS

This work was sponsored by the U. S. Department of Energy's Building Technologies Office under Contract No. DE-AC05-00OR22725 with UT-Battelle, LLC. The authors would like to acknowledge Mr. Antonio Bouza, Technology Manager – HVAC&R, Water Heating, and Appliance, US Department of Energy Building Technologies Office.